Ann. Geophys., 26, 117–129, 2008
www.ann-geophys.net/26/117/2008/

Annales Geophysicae

30 MHz radar observations of artificial E region field-aligned plasma irregularities

D. L. Hysell

Earth and Atmospheric Science, Cornell University, Ithaca, NY, USA

Received: 19 September 2007 – Revised: 22 December 2007 – Accepted: 17 January 2008 – Published: 4 February 2008

Abstract. Artificial E region field aligned irregularities (FAIs) have been observed during heating experiments at the HAARP facility using a new 30 MHz coherent scatter radar imager deployed near Homer, Alaska. Irregularities were observed during brief experiments on three quiet days in July and August, 2007, when the daytime E region critical frequency was close to 3 MHz. Irregularities were consistently generated and detected during experiments with O-mode HF pumping on zenith with a 1-min on, 1-min off CW modulation. The scattering cross sections, rise, and fall times of the echoes were observed as well as their spectral properties. Results were found to be mainly in agreement with observations from other mid- and high-latitude sites with some discrepancies. Radar images of the irregularity-filled volume on one case exhibited clear variations in backscatter power and Doppler shift across the volume. The images furthermore show the emergence of a small irregularity-filled region to the south southwest of the main region in the approximate direction of magnetic zenith.

Keywords. Ionosphere (Active experiments; Auroral ionosphere; Ionopsheric irregularities)

1 Introduction

A signature feature of ionospheric modification experiments is the production of small-scale field-aligned plasma density irregularities (FAIs) near the reflection height (see Robinson, 1989; Frolov et al., 1997 for reviews.) These irregularities give rise to coherent radar backscatter that can be detected by appropriately located low-power HF and VHF radar systems (e.g. Senior et al., 2004). The first coherent scatter observations were made at the Platteville site in Colorado using a variety of diagnostic wavelengths between 1–10 m (e.g. Minkoff and Kreppel, 1976, Radio Science, 9(11)). Subsequent observations of artificially induced FAIs were made in conjunction with heater experiments at Sura in Russia (e.g. Belenov et al., 1977), Arecibo (e.g. Coster et al., 1985), the EISCAT heater near Tromsø (e.g. Stubbe et al., 1982; Hedberg et al., 1983), SPEAR (e.g. Robinson et al., 2006), and at the emerging HAARP site near Gakona, Alaska (Hughes et al., 2003). Observations at different radar and heating frequencies and at different latitudes and pointing directions have spurred controversy and accelerated the development of comprehensive ionospheric modification theories.

Most of the research in this area has focused on artificial FAIs created in the F region. F region FAIs are characterized by long decay times indicative, in part, of the background ambipolar diffusion coefficient. The Doppler shifts of the irregularities are closely related to the ambient $\mathbf{E}\times\mathbf{B}$ drift velocity and can be used to diagnose both the background electric field and also fields associated with MHD waves (e.g. Yampolski et al., 1997). Artificial F region FAIs are therefore important not only for studying heating-related phenomena but also for diagnosing aeronomic and magnetosphere-ionosphere coupling processes. At high latitudes, substantial refraction is usually required for observations of the FAIs by ground-based radars, and so HF probe waves are mainly used. Many of the relevant observations have been made with SuperDARN-class radars which can also operate on demand and not just during short campaigns (e.g. Bond et al., 1997; Eglitis et al., 1998).

By comparison, artificial FAIs created in the E region have seen relatively little investigation. Generating them necessitates either very low pump frequencies or, failing that, the presence of sporadic E layers or auroral precipitation. Planning experiments around these phenomena is challenging, and the latter can cause significant attenuation of the probing radar signal. The Platteville and Arecibo heaters operated at sufficiently low frequencies to generate E region FAIs under normal daytime conditions as well as during sporadic E events, as could the EISCAT facility in the early 1980s (Frey, 1986), but similar low-frequency heating capability has been absent until recently.

Correspondence to: D. L. Hysell
(dlh37@cornell.edu)

Published by Copernicus Publications on behalf of the European Geosciences Union.

Table 1. Coherent scatter radar characteristics for the July/August, 2007 experiments.

parameter	value
frequency	29.795 MHz
peak power	12 kW
pulse length	19.5 km
coding	13 bit Barker
duty cycle	5.27%
IPP	370 km
$h0$	40 km
δh	1.5 km
bandwidth	100 kHz
no. ranges	120
no. channels	6
data rate	2.22 MB/s

Moreover, the geographic constraints for field-aligned radar backscatter from E region FAIs are difficult to meet at auroral latitudes due to the low elevation angles involved and the minimal role playable by refraction, and specialized radars dedicated to heater support must generally be used. Hibberd et al. (1983, 1984) observed coherent backscatter from E region FAIs using the STARE radar with permanent sites in Norway and Finland suitable for supporting heater experiments at Tromsø. In a subsequent campaign, a portable 46.9 MHz radar deployed in Sweden joined the STARE radar in conducting perhaps the most extensive study of artificial E region FAIs to date (Djuth et al., 1985; Noble, 1987).

The recent completion of the HAARP ionospheric modification facility, which is able to radiate at frequencies as low as 2.75 MHz, prompts the reinvestigation of artificial E region FAIs and coherent radar backscatter from them. A new 30 MHz portable radar imager was recently installed near Homer, Alaska, to undertake the investigation. We study E region artificial FAIs no only to test existing theories for artificial irregularity generation but also to assess the effects of heating on naturally occurring auroral E region plasma waves and irregularities (e.g. Robinson et al., 1995, 1998). In this paper, we report on findings from a recent set of preliminary experiments. The 30 MHz radar is autonomous and remotely operable and will be available for more extensive studies in the near term.

2 Experiment description

For E region FAI observations over the HAARP site near Gakona (62.39 N, 145.15 W), a coherent scatter radar was installed on the southern tip of Alaska's Kenai Peninsula, across Kachemak Bay from Homer and near the small town of Seldovia. The radar was deployed at the NOAA Kasitsna Bay Laboratory (KBL) (59.47 N, 151.55 W) where extensive infrastructure exists.

Figure 1 illustrates the motivation for the coherent scatter radar siting. It represents the geomagnetic scattering geometry calculated using raytracing. For the calculations, the E region ionosphere was modeled as having a peak density of $10^5\,\mathrm{cm}^{-3}$ at an altitude of 110 km, a 5 km density scale length below the peak, and a 100 km scale length above the peak. The left panel of the figure shows the altitude of the locus of perpendicularity for monostatic backscatter from the KBL site, and the right panel shows the magnetic aspect angle (degrees off perpendicular) at an altitude of 110 km. Note that the locus of perpendicularity at 110 km for this case passes precisely over Gakona. This is the nominal altitude for auroral E region FAIs. The scattering geometry is rather sensitive to siting variations, and neither Anchorage, Kodiak, nor a bistatic link between the two would be suitable for observing E region FAIs over HAARP.

The radar is a portable coherent scatter radar interferometer operating near 30 MHz, making it sensitive to the presence of 5-m irregularities. The frequency was chosen mainly for its suitability for observing naturally occurring type 1 and type 2 field aligned irregularities associated with the aurora and also with meteor trails. The radar uses a solid-state transmitter, an arbitrary waveform generator, and digital receivers based on the Echotek ECDR-GC314PCIfs product family. Six receiver channels are presently supported.

Antenna arrays are constructed from six groups of horizontally-polarized 3-element Yagi antennas. Some are used for transmission, and all are used for reception. The transmission main antenna beam is directed toward Gakona at an elevation of 25° and has a ∼12° E-plane and ∼30° H-plane half-power beamwidth. The overall gain of the transmitting array is about 18.5 dBi. For reception, the six antenna groups are spaced so as to form 15 nonredundant interferometry baselines, the longest with a length of almost 8 wavelengths transverse to the direction of transmission. Table 1 lists the most important characteristics of the radar. Note that the range to the E region over Gakona is approximately 480 km and therefore greater than the nominal 370 km interpulse period (IPP). Echoes will therefore be range aliased and appear in range bins in the neighborhood of 110 km.

The radar is an imaging radar similar to the one deployed near Anchorage for auroral investigations (Bahcivan et al., 2005) and in the Caribbean for sporadic E layer studies (Hysell et al., 2004). Data can be processed using the principles of synthetic aperture radar imaging which were thoroughly examined recently by Hysell and Chau (2006). Radar imaging affords the possibility of examining spatial fine structure in the modified volume over HAARP relatively free of spatio-temporal ambiguity. The imaging algorithm in use can be considered a super-resolution method and is not diffraction limited.

Experiments were conducted on 28, 30 July, and 2 August 2007. In each case, the entire HAARP facility was used

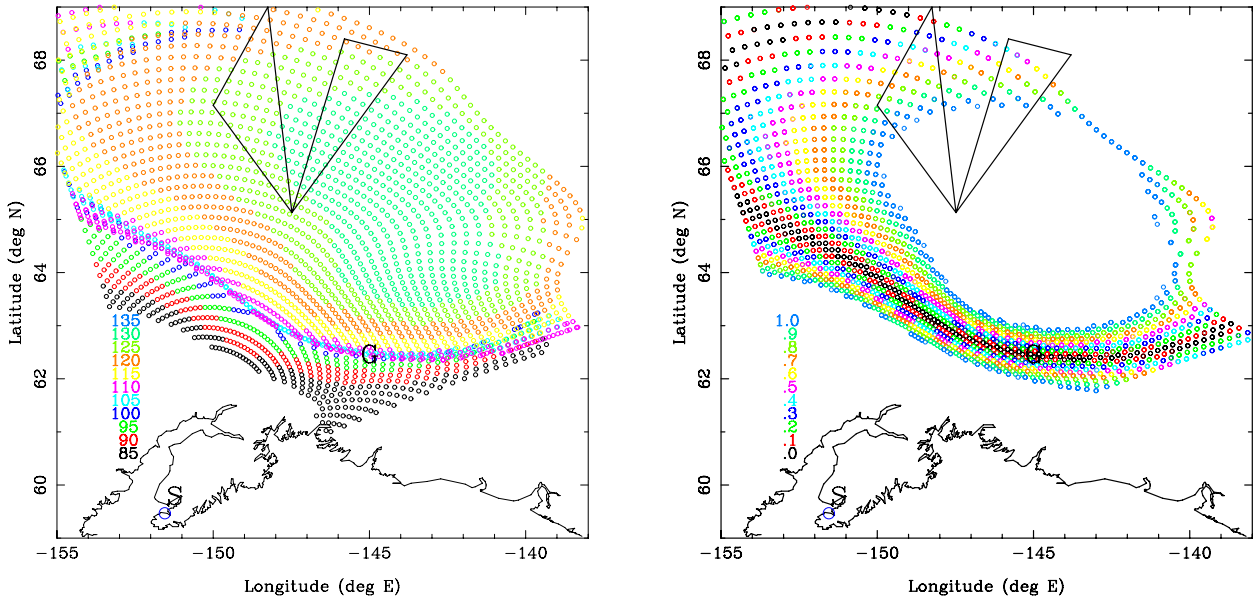

Fig. 1. Raytracing calculation for 30 MHz radar signals emanating from the KBL site near Seldovia, Alaska (plotter symbol "*S*"). Left panel: altitude of the locus of perpendicularity in km. Right panel: magnetic aspect angle at an altitude of 110 km in degrees. The Gakona site is indicated by the plotter symbol "*G*". The triangles represent flight corridors for the Poker Flat Rocket Range, which are shown as an indication of scale.

to transmit O-mode signals in the zenith direction on a 1-min on, 1-min off schedule. The heating frequency was 2.75 MHz except on 2 August when it was 3.25 MHz. The effective radiated power and half-power beamwidth for HAARP at these frequencies are between about 86–88 dBW and ∼15°, respectively. In every case, observations were made in the daytime when background E layer ionization was present. The E layer critical frequency was regular and slowly varying.

Figure 2 shows the E region critical frequency measured over HAARP by the facility Digisonde throughout the week of the experiments in question. The value of FoE demonstrated a regular diurnal cycle with a midday peak at approximately 3 MHz. Note that local UTC=SLT+9 h and that the peaks occurred near local noon. There was no precipitation, and absorption did not affect the radar diagnostics. There were no significant sporadic E layers during the time of our experiments.

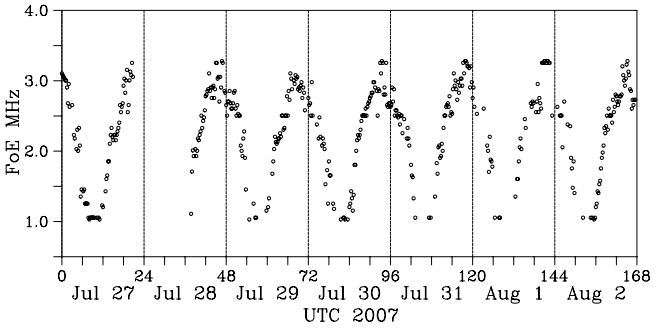

Fig. 2. FoE for the week of the E region FAI experiments measured by the HAARP Digisonde.

3 Observations

Radar observations for 30 July 2007 are shown in Fig. 3. The heating frequency of 2.75 MHz was well below the E region critical frequency of 3.0 MHz at this time. Data from all six receiver channels were combined to construct this figure and the others like it in the paper. The data were incoherently integrated (power averaged) for ∼3 s to make this figure. This is a so-called range-time-Doppler-intensity plot, in which the brightness of the plotted pixels conveys the signal-to-noise ratio, the hue conveys the Doppler shift, and the saturation conveys the Doppler width. A similar plotting style is followed in Figs. 4, 6, and 8 that follow. Signal-to-noise ratios between −10–30 dB are depicted here. The data have been coherently integrated (voltage averaged) by a factor of 4, and Doppler velocities between ±253 m/s are represented, with positive velocities (blue shifts) implying motion toward the radar.

The strongest features in Fig. 3 occur mainly in range bins above 90 km and are associated with a combination of specular and non-specular meteor trail echoes. The near absence of meteor trail echoes at apparent ranges less than 90 km suggests that the echoes are not range aliased and that their apparent range is the true range. The Doppler shifts of the meteor echoes are presumably related to the line-of-sight wind

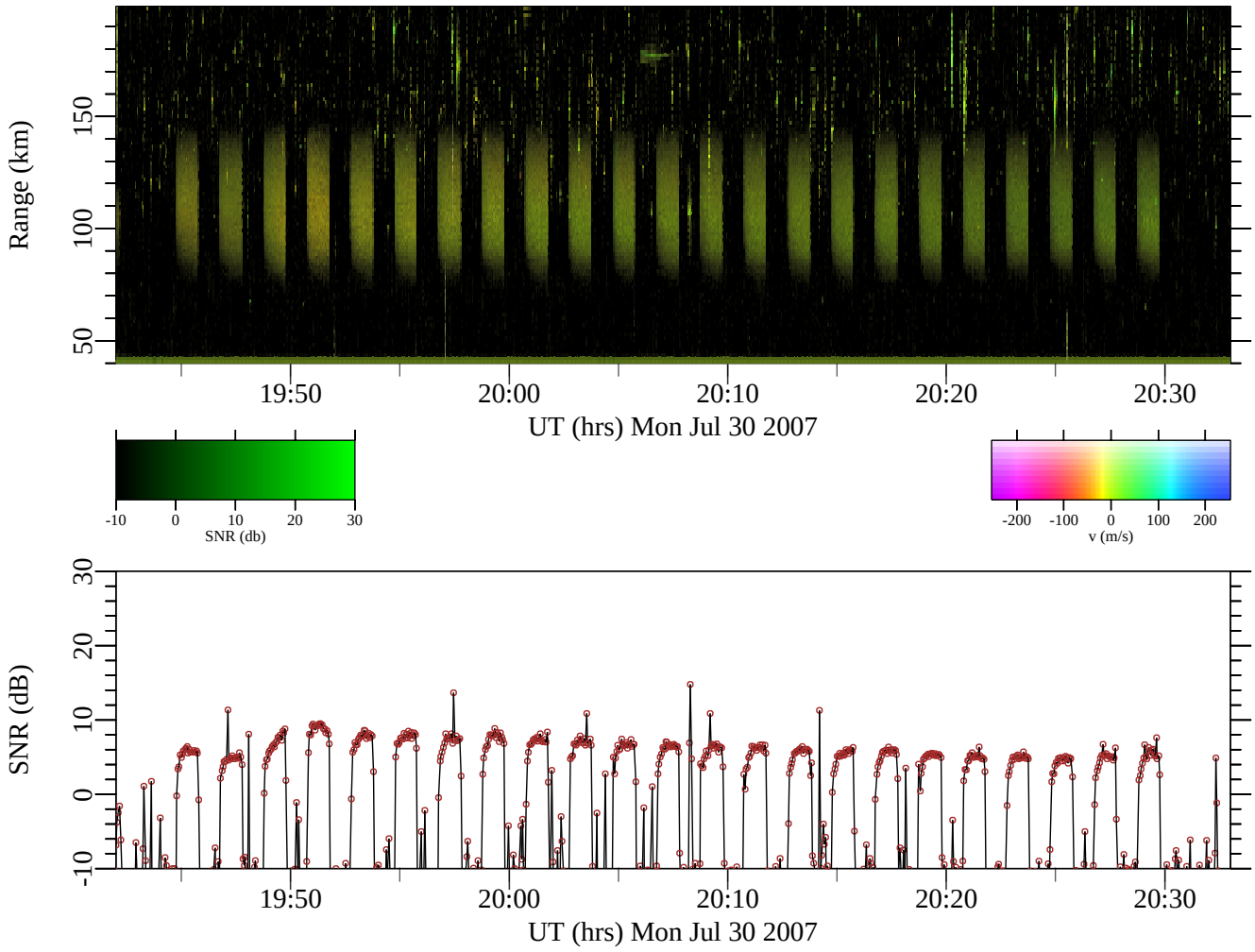

Fig. 3. RTDI plot of backscatter from artificial E region FAIs over HAARP observed on 30 July 2007. Note that the echoes from heater-induced FAIs are range aliased and that their true range is greater than their apparent range by 370 km. The signal-to-noise ratio for apparent ranges between 90–130 km is plotted beneath the RTDI plot. Note also the tendency for meteor echoes to obscure artificial E region FAIs.

speed at the site of the trail. While we have observed meteor echoes with Doppler shifts as great as about ±200 m/s during other experiments, the Doppler shifts shows here are all less than 50 m/s, and most are less than 20 m/s. It is not uncommon to observe intense, long-lived range-spread meteor trails in the 30 MHz radar data with lifetimes of several minutes and signal-to-noise ratios well in excess of 30 dB. Their interpretation is the subject of another report, however.

Of greatest interest here are the regular bands of backscatter between 80–140 km apparent range. These represent backscatter from artificial E region field aligned irregularities over HAARP. They are range aliased and so have true ranges between 450–510 km. Note that echoes at this range arrive with elevation angles of only about 10° where the gain of the antennas is reduced by 3–4 dB from the maximum. The echoes here have signal-to-noise ratios as great as about 10 dB. Their range extent grows with time each time the heater is turned on and also exhibits gradual variation over the course of the experiment. The echoes have small Doppler shifts and are slightly red-shifted in the first few bands. There is some variation in Doppler shift with range, with the largest red shifts occurring in the middle of the bands. Their Doppler widths are much smaller than the sample bandwidth here (see below).

The lower panel of Fig. 3 shows the signal-to-noise ratio in ranges between 90–130 km. This is the span of ranges completely occupied by irregularities throughout the entire 1-min heating intervals. The plot suggests a broad envelope for the backscatter intensity, which increases early in the experiment and then decreases more slowly. Furthermore, each heating interval seems to undergo a regular cycle, beginning with a ∼3 dB intensification period lasting 20–30 s followed by a period of roughly constant intensity. The envelope sometimes acts to obscure the regular cycle, however.

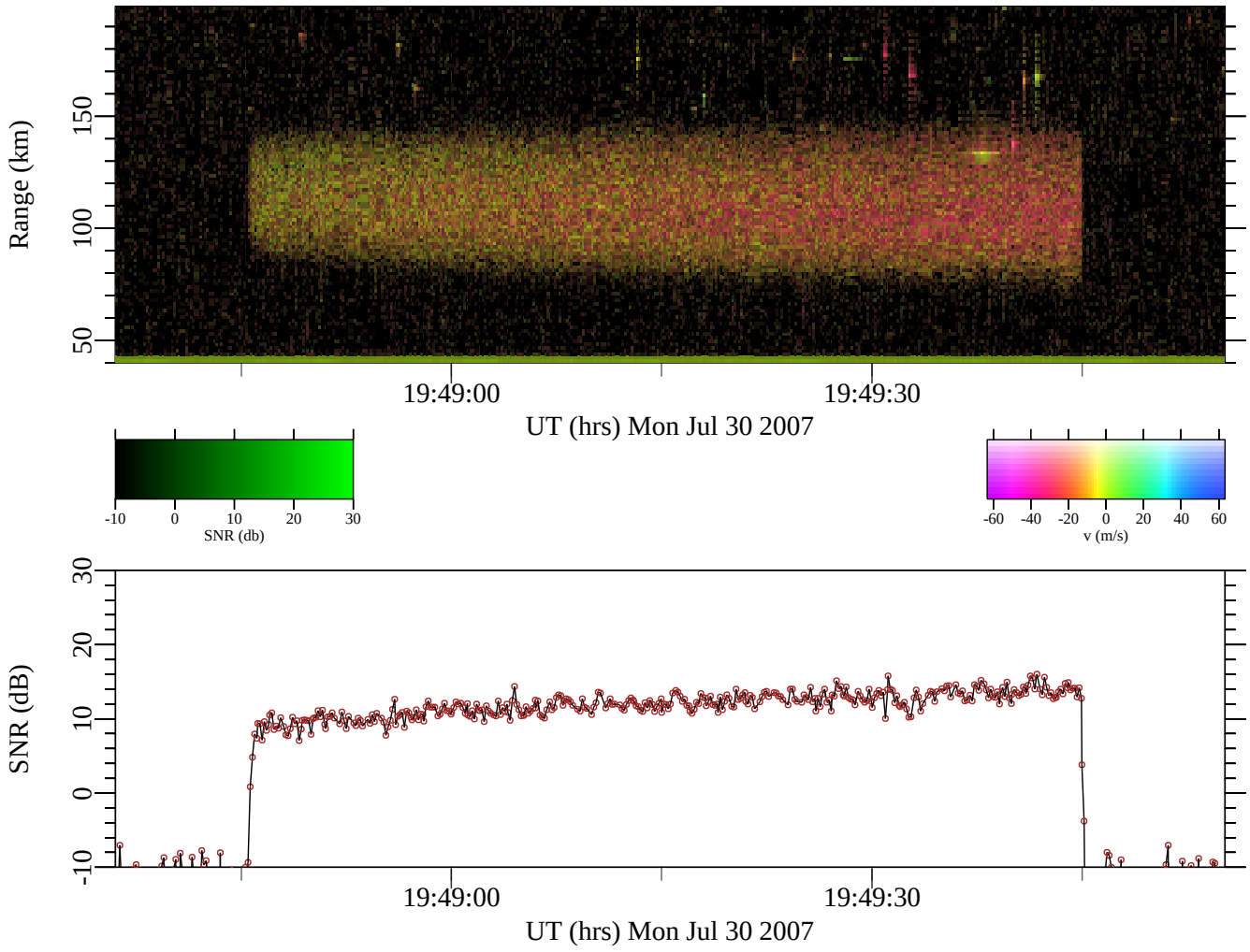

Fig. 4. Close-up view of one of the backscatter bands from the previous figure. The signal-to-noise ratio for apparent ranges between 90–130 km is plotted beneath the RTDI plot.

The broadening and redshift of the first few backscatter bands in the upper panel of Fig. 3 occurs simultaneously with the intensification seen in the lower panel.

One of the bands of backscatter is examined in more detail in Fig. 4. This time, the data were coherently integrated by a factor of 16 and incoherently integrated for an interval of 0.158 s (or four contiguous samples). This expanded figure exemplifies a number of features of the backscatter from the artificial FAIs. These include the tendency for the the near and far edges of the scattering region and the near edge in particular to expand from the center over time. The backscatter intensity also appears to increase throughout the scattering region over time. In this example, the Doppler shifts become increasingly negative (red shifted) over time, with the most negative Doppler shifts occurring at ranges in the middle of the region. Finally, the echoes turn on and off almost simultaneously over wide range spans.

The lower panel in the figure shows a gradual increase in scattering intensity across the interval. The panel also reveals the rise and fall times of the scattered signal during heater turn-on and turn-off. Those times are of the order of 0.5 s and are comparable. The corresponding e-folding time is about 100 ms.

A more precise determination of the times based on one heating interval is complicated by the presence of significant temporal fluctuations in the backscatter intensity. These fluctuations are at least partially deterministic and appear to be well correlated over a timescale of about 1 s. In view of the fact that approximately 100 statistically independent power estimates contribute to each point in the lower panel of Fig. 4, we would expect statistical fluctuations at the level of 10% RMS in the signal power or about ± 0.5 dB. (Since the signals from the six receiver channels are highly correlated, averaging them introduces no drastic improvement in the statistical confidence.) The actual fluctuation level during heating events is significantly greater (1–2 dB).

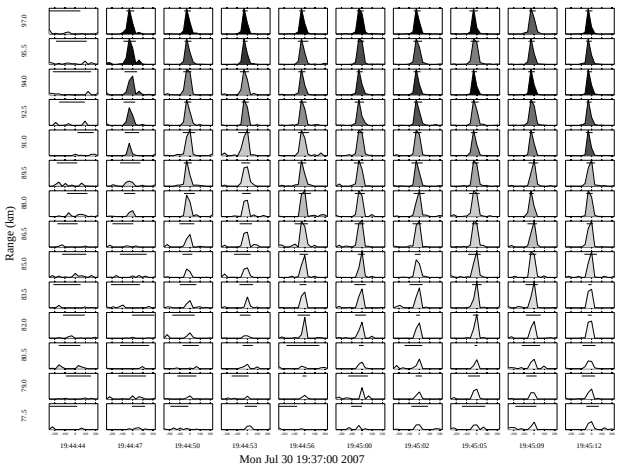

Fig. 5. Doppler spectra computed during the early part of a heating event. The gray levels represent relative signal intensity on a per column basis.

Doppler spectra corresponding to the beginning of a heating interval on 30 July are shown in Fig. 5. As in Fig. 3, these data were coherently integrated by a factor of 4 and incoherently integrated for approximately 3 s. Doppler velocities span ± 253 m/s. The spectra of fully-developed scattering regions have half power widths mainly between 50–80 m/s and exhibit small variations in range and time. Spectra from regions undergoing intensification are broader. The spectra show clearly how the scattering regions at shortest range turned on approximately 10 s after the regions at greater distance.

Figure 6 shows data similar to those in Fig. 3 except collected on 28 July 2007, after 23:00 UT, when FoE had decreased to about 2.7–2.8 MHz. The heating frequency remained 2.75 MHz — comparable to the critical frequency but still well below the peak upper hybrid resonance frequency ($\omega_{uh}^2 = \omega_p^2 + \omega_c^2$). These data were also coherently integrated by a factor of 4 and incoherently integrated for approximately 3 s. The signal-to-noise ratios shown here are 4–10 dB less than those in Fig. 3 and do not exhibit a gradual modulation envelope. The range extents of the different strips also appear to undergo no gradual variations, and the Doppler shifts are likewise uniform and small.

However, the echoes depicted in Fig. 6 exhibit clearer short-term intensity variations than did those in Fig. 3. The echoes here intensify throughout the first half of the heating intervals at a rate of about 3 dB/20–30 s. The intensification timescales and saturation times were consistent throughout the experiment. Similar behavior might also be present in Fig. 3, only there it is obscured by the gradual modulation envelope.

Some of the aforementioned phenomena can be elucidated with the aid of radar imaging, which permits the sorting of radar data by range, Doppler shift, and also bearing. In aperture synthesis imaging, a large, steerable antenna is synthesized from small, fixed antenna groups appropriately situated on the ground, and true images of the radar scatter are constructed, one range and Doppler frequency at a time. The technique, which derives from the field of radio astronomy, was recently reviewed by Hysell and Chau (2006). We use a Bayesian methodology to transform cross-spectral data (radar visibilities) to images of backscatter power versus bearing (radar brightness). We apply it here for the first time to the study of artificial E region FAIs.

While the radar images produced are inherently three-dimensional, small uncertainties in elevation angle (or more specifically the associated direction cosine) translate into large uncertainties in altitude, particularly at polar latitudes. Emphasis will therefore be placed here on calculating two-dimensional images in range and azimuth, which can then be translated to latitude and longitude. Extracting estimates of the scatterer altitudes from the interferometry data will be the subject of future investigations.

Figure 7 shows a sequence of radar images generated throughout a heating interval in the 30 July 2007 dataset. Contours indicate the altitude of the locus of perpendicularity at different altitudes, neglecting the effects of refraction. The "P", "F", and "+" plotter symbols denote the locations of Poker Flat, Fairbanks, and HAARP. Seldovia falls off the bottom boundary of the images.

Data were once again processed with a factor of 4 coherent integration followed by incoherent integration for 3 s. Separate images were constructed for each of 16 Doppler frequency bins and then combined graphically. Backscatter intensity, Doppler shift, and spectral width are once again represented by the brightness, hue, and saturation of the pixels in the images as shown in the legend. Images are divided into 128 azimuth bins, each about 0.7° or about 5.9 km wide over Gakona. Since the backscatter is concentrated in just a few azimuth bins, the signal-to-noise ratio in those bins is increased, much as it is increased through coherent processing when it occupies just a few spectral bins. The signal-to-noise ratios depicted in Fig. 7 approach 30 dB at times.

The earliest image from 19:48:47 is the first one with detectable content after heater turn-on. The image shows a ragged region of weak scatter appearing above HAARP. Three seconds later, the modified region has expanded, intensified, and rounded out. The backscatter intensity is strongest in the center of the region, but the Doppler velocity is essentially uniform. By 19:49:02, the modified region is showing two new characteristics. The first is a variation in the Doppler frequency, with a red-shifted region appearing in the northwest corner of the modified volume. The second is a new scattering region appearing outside and to the south southwest of the main round one. This region typically appears $\sim$10 s after the main one in all of the heating intervals. Since the new echoes occur in the shortest range gates, their appearance is related to the expansion of the echo range span on the near side.

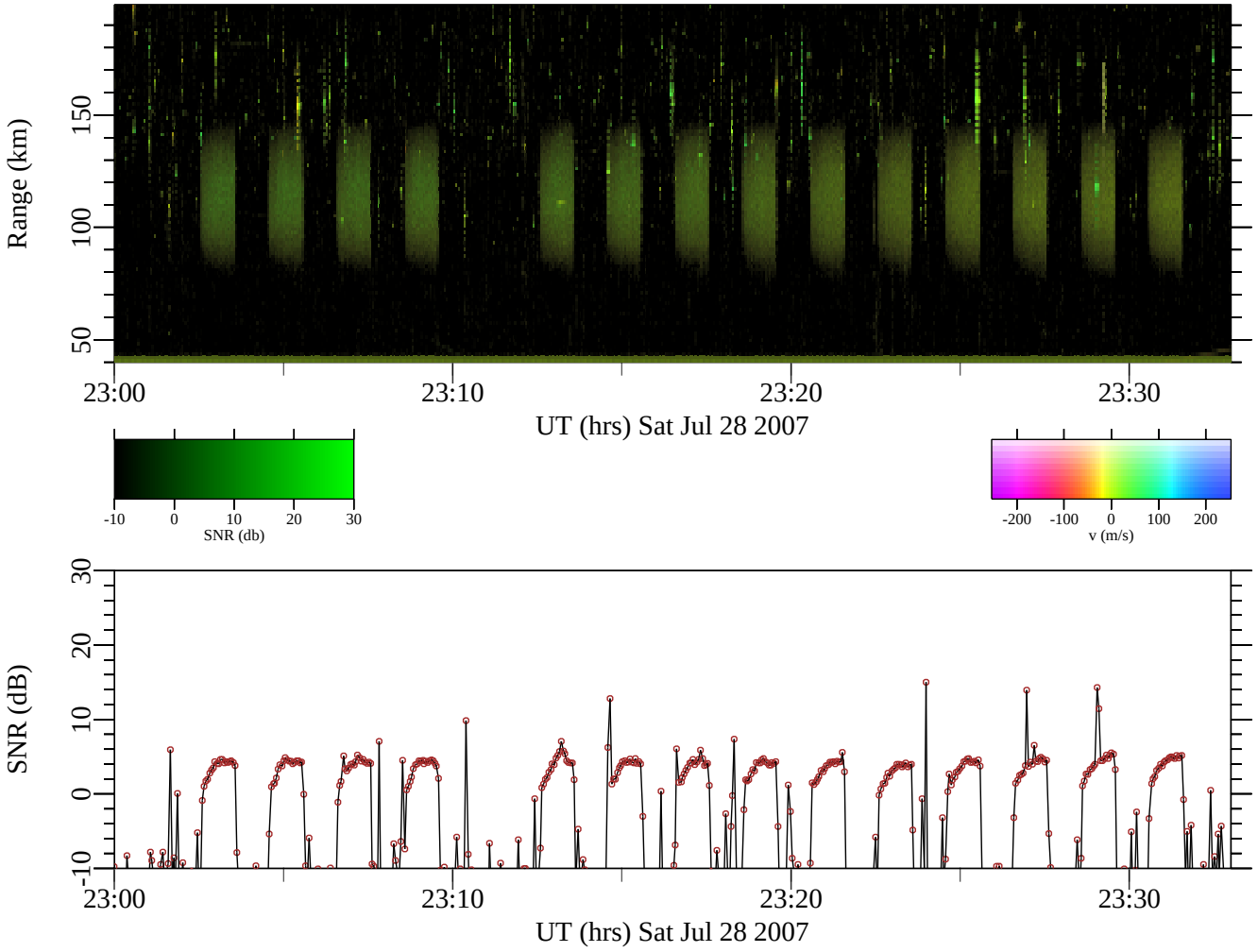

Fig. 6. RTDI plot for 28 July 2007. Note that ionospheric modification was interrupted during the gap around 23:18 UT. The lower panel shows the signal-to-noise ratio for echoes between 100–130 km.

By 19:49:12, both the main scattering region and the satellite region have intensified, although a clear boundary continues to delineate them. The red-shifted region in the northwest quadrant has grown more distinct. The images remain essentially identical after this time, although some fine structure in the power and Doppler shifts appears to come and go.

Similar sequences of events can be seen in animated imagery of the entire 30 July experiment. The July 28 experiment also produced comparable images, except that the Doppler shifts are uniform and small over time and across the entire modified region. The smaller scattering region to the south southwest of the main one occurs universally, always appearing after a ∼10 s delay.

Finally, we note that backscatter from artificial FAIs was detected during a brief experiment on 2 August when the heater frequency (3.25 MHz) was above the E region critical frequency at the time (∼3 MHz) and close to the upper-hybrid resonance frequency at the peak. The results for the first 10 min. of that experiment are shown in Fig. 8. These data were processed using 4 coherent integrations and incoherent integration for 3 s. The backscatter was weak, with a maximum signal-to-noise ratio of only about 3 dB. The Doppler shifts are uniform and small. Most remarkably, the growth time for the irregularities has increased dramatically compared to the earlier examples. From Fig. 8, a growth period of approximately 1 e-fold in 4 s. can be estimated. This period was consistent throughout the entire experiment, which lasted for about 25 min. Some but not all of the heating events also exhibited the gradual (3 dB in 30 s) growth phase during the first ∼20–30 s of the heating interval.

Radar images of the irregularities created on 2 August are qualitatively similar to those shown earlier, except that there was no obvious spatial structure in the Doppler shifts. The images were fainter but showed the same main circular

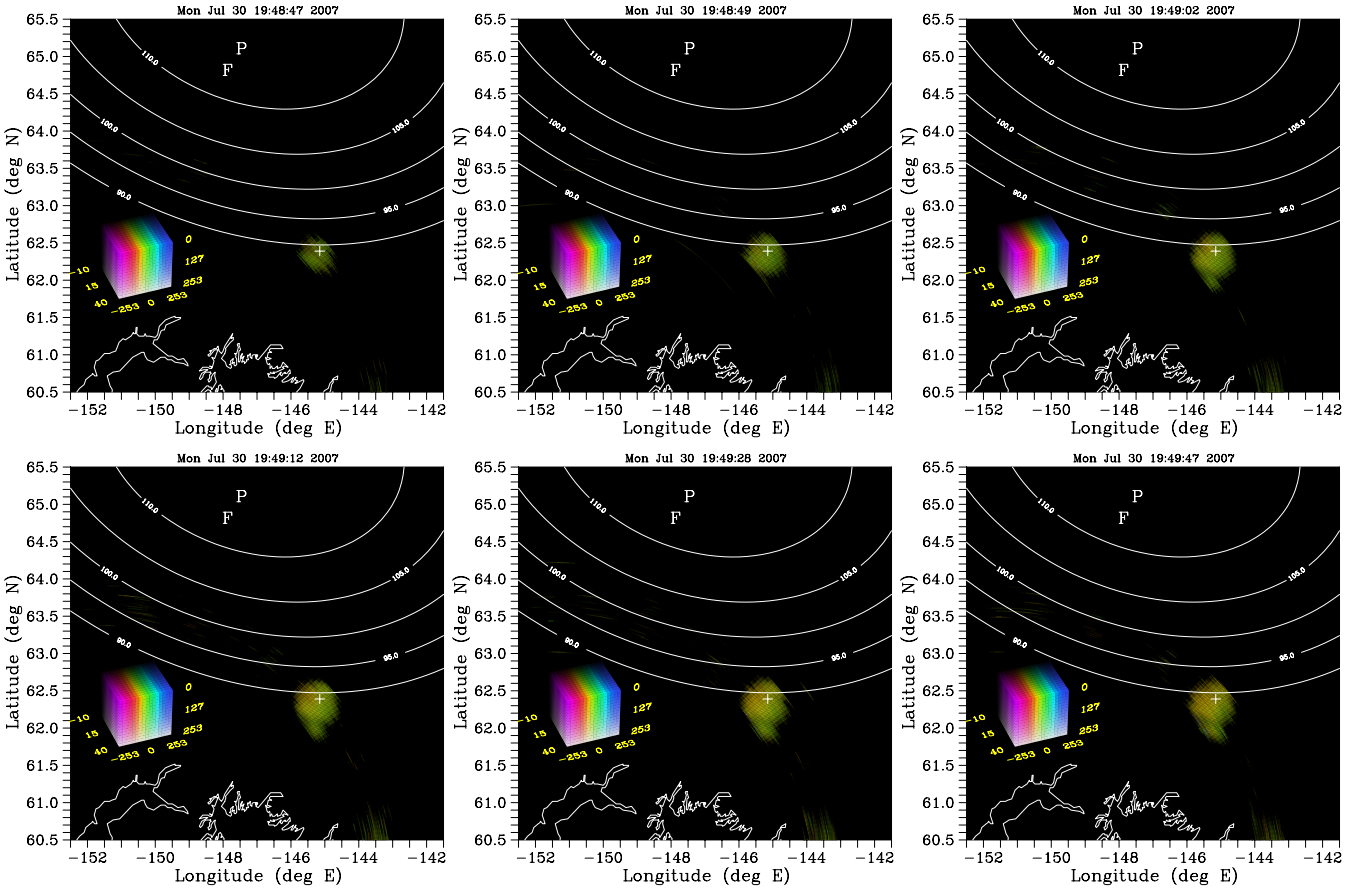

Fig. 7. Radar images illustrating the temporal evolution of artificial E region FAIs in the heater-modified volume. Contours mark the locus of perpendicularity in the absence of refraction. The HAARP site is indicated by the "+" symbol. The color legend associates pixel brightness, hue, and saturation with signal-to-noise ratio (−10–40 dB), Doppler shift (±253 m/s), and spectral width (0–253 m/s), respectively.

scattering region with a satellite region to the south southwest. The smaller scattering region developed very slowly and is only clearly visible in the images about 20 s after heater turn-on.

4 Analysis

Artificial FAIs are generally believed to be generated by thermal parametric instabilities (TPIs) which form at altitudes slightly above the upper hybrid resonance height where the pump frequency is the Pythagorean sum of the plasma frequency and the electron gyrofrequency (Grach et al., 1977; Das and Fejer, 1979; Grach et al., 1981; Dsythe et al., 1982; Dsythe et al., 1983). In the nonlinear stage of evolution, the TPI goes over to the resonance instability developed by Vas'kov and Gurevich (1975, 1977) and expanded upon by Inhester (1982). Evidence that E region FAIs are caused by TPIs was presented by Djuth et al. (1985) on the basis of threshold heating power and frequency and irregularity growth time arguments, although Noble (1987) argued that a number of other candidate mechanisms could not be ruled out. The present objective is to match theoretical predictions for TPIs and other instability mechanisms with observations.

In summary, the salient features of the July/August 2007 experiments are

1. The creation of artificial E region field aligned irregularities in a circular region above the heater with a diameter expanding to more than 50 km. Note that the HAARP ERP is down by from 9–14 dB at the periphery of this region.
2. A timescale for turn-on of the order of 100 ms in the case of strong irregularities created by heating below FoE and of the order of 4 s for weaker irregularities and heating above FoE but near the upper-hybrid resonance.
3. A timescale for turn-off of the order of 100 ms.
4. Simultaneous turn-on and turn-off across broad range spans.
5. Slow expansion and intensification of the irregularity region by about 3 dB during the first 20–30 s.

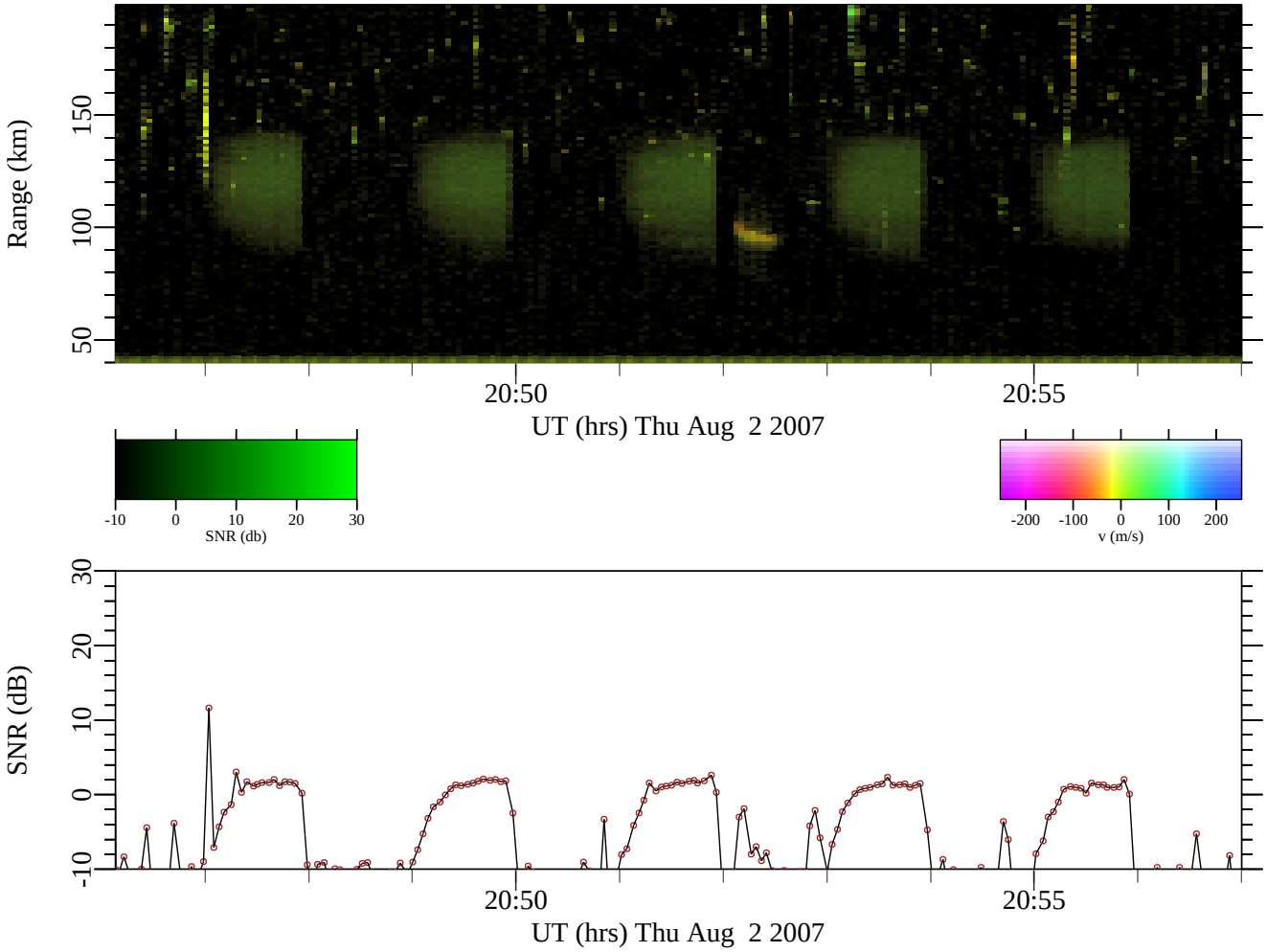

Fig. 8. RTDI plot for 2 August 2007. The lower panel shows the signal-to-noise ratio for echoes between 110–130 km.

6. Doppler spectra exhibiting small Doppler shifts and spectral half-power widths of the order of 50–80 m/s.

7. The creation of FAIs in a small region to the south southwest of the main modified region appearing 10–20 s after the main region.

8. An occasion when the size, intensity, and Doppler shift of the modified region appeared to undergo simultaneous, long-term modulation. On this occasion, the Doppler shifts within the modified region were inhomogeneous in a manner suggesting circulation.

The HAARP antenna is an array of 15×12 broadband elements aligned 14° E of N. The half-power full beamwidth (HPFB) of the pattern in the E-W and N-S planes is about 15°×18° at 2.75 MHz and 12°×15° at 3.25 MHz. The corresponding diameter of the illuminated E region (about ∼30 km) is comparable to the size of the irregularity filled region during the first few seconds of heating but much smaller than its 50+ km terminal diameter. Better correspondence to the latter size is found by comparing the bright regions in the images with the beamwidth to the first null (BWFN) of the HF antenna, which approximately twice the half-power beamwidth (HPBW). (In view of the fact that the radar images span 40 dB of dynamic range, the HPBW may be essentially irrelevant.) However, the absence of a complete, clearly defined heater sidelobe pattern in the radar images indicates that the heater radiation pattern by itself does not determine the size and shape of the irregularity filled region.

We may expect the irregularity-filled region to be influenced by the Spitze angle θ_c, the upper bound on the zenith angle of an O-mode ray launched from the ground that will reach the reflection height in a stratified ionosphere. It is calculated by combining Snell's law with the largest index of refraction a ray can have at the reflection height. Here, θ_c=arcsin($\sqrt{\frac{f_c}{f_c+f_\circ}}\sin\chi$)=8.55° given a heater frequency $f_\circ$=2.75 MHz, an electron gyrofrequency

f_c=1.5 MHz, and a magnetic zenith angle χ=14.0°. The associated spot size at an altitude of 110 km is about 32 km. A somewhat larger region (about 40 km diameter) is anticipated if the rays need only penetrate to the upper hybrid resonance altitude for FAI generation. Djuth et al. (1985) observed the spreading of artificial FAIs well outside the Spitze angle and attributed this to imperfect density stratification and horizontal density gradients associated with an active aurora altering the refraction. While there was no auroral activity during the present experiments, the expansion of modified region over time suggests that heater-induced variations in plasma density (self focusing) could have played an analogous role in expanding the irregularity-filled region over intervals of tens of seconds.

The greater the difference between the upper hybrid resonance frequency at the E layer peak and the HF heating frequency, the greater the intensity of the coherent scatter in our experiments. This may be indicative of the depth of the FAI production region, but it should also be noted that the ability for the 30 MHz probe signal to satisfy the condition for field aligned backscatter is degraded when the critical frequency is low. On the basis of the radar characteristics and using a hard-target (non beam filling) formulation, the total scattering cross section for the strongest of the echoes observed in the July/August experiments can be estimated at about 6×10^5 m^2. This is comparable to estimates obtained at Platteville for artificial E region FAIs, which were characterized as falling between 50–65 dBsm over a broad range of probe frequencies below 110 MHz (Fialer, 1974). The figures obtained by Noble (1987) from observations at Tromsø at 143.8 MHz and 46.9 MHz were 10^5 m^2 and 10^4 m^2, respectively, where the reduced value at VHF was tentatively attributed to auroral precipitation and absorption. Scattering cross sections have been reported to saturate at heating power levels in the range of 130–190 MW ERP (Noble, 1987) (see also Hedberg et al. (1983, 1986)). Power levels in the present experiment were always well above that saturation threshold.

The Doppler shifts reported here are all much smaller than those presented by Noble (1987) who interpreted them in terms of the background convection speed. In their experiments at Tromsø, the Doppler shifts and spectral widths measured simultaneously at 21.4 and 46.9 MHz were consistent when interpreted as velocities (i.e. the frequencies scaled with wavenumber). They reported 110 m/s line-of-sight Doppler shifts and half-power Doppler widths of 5–11 Hz (35–77 m/s) at 21.4 MHz and 12–20 Hz (38-64 m/s) at 49.6 MHz The half-power spectral widths reported here for fully-developed scattering regions of ∼10–16 Hz (∼50–80 m/s for 30 MHz) therefore fit neatly between the results from Tromsø. Djuth et al. (1985) attributed their observed spectral width, in part, to the rapid background flow and the possible effect of beam broadening. There is no suggestion of strong auroral convection in the data from Alaska, however. The HAARP site is typically sub-auroral, and natural auroral activity occurs infrequently overhead.

Noble (1987) reported echo rise and fall times of the order of hundreds of ms for what they termed "type A" artificial E region FAIs. Comparing observations at 21.4, 46.9, and 143.8 MHz, they showed that the rise and fall times scaled approximately with the probe wavelength and the square of the probe wavelength, respectively. The former is expected for the linear growth rate of the thermal parametric instability according to Grach et al. (1978), and the latter for ordinary transverse ambipolar diffusion. The ∼100 m/s rise and fall times for the 30 MHz echoes shown here fall between those reported for 46.9 and 143.8 MHz probe signals by Noble (1987) and are also shorter than the decay times reported by Coster et al. (1985) for 50 MHz echoes at Arecibo (although not the rise times), in at least partial defiance of the scaling laws. The rapid variation in the electron collision frequency with altitude would seem to permit a wide variance in timescales depending on the altitude of the irregularities, however.

Noble (1987) also observed artificial FAIs with growth timescales 10 or more times longer than the type A irregularities. These they termed "type B". This classification appears to apply to the 2 August event when the artificial FAIs exhibited growth times of about 4 s. Noble (1987) links the type B irregularities with gradient drift instability. If this were the case, we would expect the Doppler shifts of the irregularities to vary from one side of the modified region to the other. While this behavior was observed during the 30 July experiment, it was not observed on 2 August.

Noble (1987) did not observe the third timescale reported here: the gradual, systematic intensification and broadening of the echoes over intervals of tens of seconds. This phenomenon has been reported in experiments at Platteville, where it was associated with the "cold turn-on" of the heater (Frank, 1974) (see Djuth et al., 1985). The cold turn on has also been observed at Arecibo, but only rarely (Coster et al., 1985). It may be that rapid fading and structuring associated with auroral activity could have obscured the cold turn-on in experiments at Tromsø, whereas it did not do so here. The long timescale of the cold turn-on suggests a self-focusing phenomenon, where irregularity formation permits the upper hybrid matching condition to be met more easily over an increasingly large volume.

The small satellite scattering region to the south-southwest of the main region lies at the edge of the main lobe of the HF transmitter, precisely at the location of the first null. It is well outside the Spitze angle and just beyond the 14.0° magnetic zenith angle. The south southwestward displacement of the satellite region suggests two possible explanations for its source. The first is that the HF O-mode signal coupled into the Z mode at the Spitze. The Z-mode radiation then propagated horizontally and magnetic southward until encountering the southern edge of the intermediate-scale plasma striations that occupy the modified region. There, they generated small scale artificial FAIs by the same mechanism as in the main irregularity region. The ∼10 s turn-on time could

correspond to the time it takes for the density cavity in the E region to form.

Another possibility is that the satellite irregularity region is related to heating at magnetic zenith through the HF heater sidelobe. Considerable interest has been devoted lately to ionospheric modification effects at magnetic zenith (Isham et al., 1999; Pedersen et al., 2003; Rietveld et al., 2003; Mishin et al., 2004, 2005; Djuth et al., 2005). At magnetic zenith, electron heating, HF-induced airglow, and the production of ion acoustic waves are all enhanced. The process begins with the generation of upper-hybrid/electron Bernstein waves through the parametric decay of the HF pump wave and can occur well below the HF reflection height (Mishin et al., 2004, 2005). Upper-hybrid waves can also be generated through the linear mode conversion of the pump wave in the vicinity of existing density striations (Mishin et al., 2004, 2005). Upper hybrid wave trapping within the striations leads to ohmic heating, deepening of the striations, and thermal parametric instability (Grach et al., 1981; Dsythe et al., 1982). Subsequent wave growth leads to explosive growth through resonance instability (Vas'kov and Gurevich, 1977).

Finally, the variation in the Doppler shift across the irregularity-filled region could be indicative of a number of phenomena besides gradient drift instability. The Doppler shifts vary from one side of the region to the other in a manner suggesting clockwise circulation. The sense is consistent with the diamagnetic drift of electrons at the the boundary of a rarefied region. It could also be consistent with the dielectric response of the region of inhomogeneous conductivity to background winds or electric fields, depending on the direction of the forcing. It is not consistent with $\mathbf{E}\times\mathbf{B}$ drifting electrons under the influence of a transverse ambipolar field, which would have the opposite sense of rotation. We can discriminate between the various mechanisms by conducting more experiments under different heating and background conditions.

5 Conclusions

This paper reports on the first observations of artificial *E* region FAIs over the HAARP facility with a new coherent scatter radar deployed near Homer, Alaska. The radar affords fine range resolution but retains sensitivity through the use of a high pulse repetition frequency and coherent integration. Using aperture synthesis techniques, it is furthermore possible to construct true images of the irregularity-filled region. Although three-dimensional imaging is possible, the present study is confined to two-dimensional analysis.

Broad similarities have been found with previous observations from Platteville and Tromsø including the echo spot size, scattering cross section, rise and fall times, and spectral width. New features have also been observed, including highly coherent fluctuations in echo power, long-term modulation of the echo intensity, extent, and Doppler shift, variations in the Doppler shift across the irregularity-filled region, and the presence of artificial FAIs to the south southwest of the main heated region. The last feature appears to be associated with the magnetic zenith direction. Future experiments involving heating along magnetic zenith should further elucidate the finding. More exhaustive observations made under a variety of heating and background ionospheric conditions should likewise allow us to quantify the features of the radar images and more closely associate them with heating instability theory.

Note that neither the 2.75 MHz nor the 3.25 MHz heating frequencies used here are close to the second electron gyroharmonic. A number of experimental studies have indicated the enhancement of certain heater-related phenomena near (mainly just above) the second gyroharmonic double-resonance (e.g. Djuth et al., 2005; Kosch et al., 2005 including FAI production and coherent scatter (e.g. Fialer, 1974; Haslett and Megill, 1974). Future experiments should provide opportunities to test this phenomenon in the E region, where naturally occurring daytime ionization is just dense enough to permit the double resonance to exist.

Acknowledgements. The author is grateful for help received from the NOAA Kasitsna Bay Laboratory, its director K. Holderied, Lab Manager M. Geagel, and Lab Director C. Geagel. The assistance of Brady O'Hanlon, Roger Varney, and G. Michhue at Cornell is also appreciated. The author is indebted to M. McCarrick for helpful input and assistance and to F. Lind and the Open Radar project. This work was supported by the High Frequency Active Auroral Research Program (HAARP) and by the Office of Naval Research under grant N00014-05-1-0748 to the University of Alaska, Fairbanks, which subcontracted Cornell. The HAARP ionosonde was developed by the University of Massachusetts, Lowell under a contract from the Air Force Research Laboratory.

Topical Editor M. Pinnock thanks M. Kosch and another anonymous referee for their help in evaluating this paper.

References

Bahcivan, H., Hysell, D. L., Larsen, M. F., and Pfaff, R. F.: 30 MHz imaging radar observations of auroral irregularities during the JOULE campaign, J. Geophys. Res., 110, A05307, doi:10.1029/2004JA010975, 2005.

Belenov, A. F., Bubnov, A., Erukhimov, L. M., et al.: Parameters of artificial small-scale ionospheric irregularities, Radiophys. Quantum Electron., 20, 1805, 1977 (engl. Transl).

Bond, G. E., Robinson, T. R., Eglitis, P., Wright, D., Stocker, A., Rietveld, M., and Jones, T.: Spatial observations by the CUTLASS coherent scatter radar of ionospheric modification by high power radio waves, Ann. Geophys., 15, 1412–1421, 1997.

Coster, A. J., Djuth, F. T., Jost, R. J., and Gordon, W. E.: The temporal evolution of 3-m striations in the modified ionosphere, J. Geophys. Res., 90, 2807–2818, 1985.

Das, A. C. and Fejer, J. A.: Resonance instability of small-scale field-aligned irregularities, J. Geophys. Res., 84, 6701–6704, 1979.

Djuth, F. T., Pedersen, T. R., Gerkin, E. A., Bernhardt, P. A., Selcher, C. A., Bristow, W. A., and Kosch, M. J.: Ionospheric modification at twice the electron cyclotron frequency, Phys. Rev. Lett., 94, 125 001-1-4, 2005.

Djuth, F. T., Jost, R. J., Noble, S. T., et al.: Observations of *E* region irregularities generated at auroral latitudes by a high-power radio wave, J. Geophys. Res., 1985.

Dsythe, K., Mjølhus, E., Pesceli, H., and Rypdal, K.: Thermal cavitons, Phys. Scr. T., 2, 548–559, 1982.

Dsythe, K., Mjølhus, E., Pesceli, H., and Rypdal, K.: A thermal oscillating two-stream instability, Phys. Fluids, 26, 146, 1983.

Eglitis, P., Robinson, T. R., Rietveld, M. T., Wright, D. M., and Bond, G. E.: The phase speed of artificial field-aligned irregularities observed by CUTLASS during HF modification of the auroral ionosphere, J. Geophys. Res., 103, 2253–2259, 1998.

Fialer, P. A.: Field-aligned scattering from a heated region of the ionosphere – Observations at HF and VHF, Radio Sci., 9, 923–940, 1974.

Frank, V. R.: E-region scatter observed at Haswell, Colorado, in Proceedings of the Prarie Smoke V RF Measurements Data Workshop, p. 75, Stanford Research Institute, Menlo Park, Calif., 1974.

Frey, A.: The observation of HF-enhanced plasma waves with the EISCAT/UHF-radar in the presence of strong Landau-damping, Geophys. Res. Lett., 13, 438–441, 1986.

Frolov, V. L., Erukhimov, L. M., Metelev, S. A., and Sergeev, E. N.: Temporal behavior of artificial small-scale ionospheric irregularities: review of experimental results, J. Atmos. Sol. Terr. Phys., 18, 2317–2333, 1997.

Grach, S., Mityakov, N., Rapoport, V., and Trakhtengertz, V.: Thermal parametric turbulence in a plasma, Physica, D, 2, 102–106, 1981.

Grach, S. M., Karashtin, A. N., Mityzkov, N. A., Rapoport, V. O., and Trakhtengerts, V. Y.: Parametric interactions between electromagnetic radiation and ionospheric plasma, Radiophys. Quantum Electron., 20, 1254–1258, 1977 (engl. Transl.).

Grach, S. M., Karashtin, A. N., Mityzkov, N. A., Rapoport, V. O., and Trakhtengerts, V. Y.: Theory of thermal parametric instability in an inhomogenous plasma, Sov. J. Plasma Phys., 4, 737–741, 1978 (engl. Transl.).

Haslett, J. C. and Megill, L. R.: A model of the enhanced airglow excited by RF radiation, Radio Sci., 9, 1005–1019, 1974.

Hedberg, Å., Derblom, H., and Thidé, B.: Observations of HF backscatter associated with the heating experiment at Tromsø, Radio Sci., 18, 840–850, 1983.

Hedberg, Å., Derblom, H., Hamberg, G., Thidé, B., Kopka, H., and Stubbe, P.: Measurements of HF backscatter cross section for striations created by ionospheric heating at different power levels, Radio Sci., 21, 117–125, 1986.

Hibberd, F. H., Nielsen, E., Stubbe, P., Kopka, H., and Rietveld, M. T.: Production of auroral zone *E* region irregularities by powerful HF heating, J. Geophys. Res., 88, 6347–6351, 1983.

Hibberd, F. H., Nielsen, E., Stubbe, P., Kopka, H., and Rietveld, M. T.: Correction to "Production of auroral zone *E* region irregularities by powerful HF heating", J. Geophys. Res., 89, 11 061–11 062, 1984.

Hughes, J. M., Bristow, W. A., Parries, R. T., and Lundell, E.: SuperDARN observations of ionospheric heater-induced upper hybrid waves, Geophys. Res. Lett., 1185, doi:10.1029/2003GL018772, 2003.

Hysell, D. L. and Chau, J. L.: Optimal aperture synthesis radar imaging, Radio Sci., 41, RS2003, doi:10.1029/2005RS003383, 2006.

Hysell, D. L., Larsen, M. F., and Zhou, Q. H.: Common volume coherent and incoherent scatter radar observations of mid-latitude sporadic *E*-layers and QP echoes, Ann. Geophys., 22, 3277–3290, 2004.

Inhester, B.: Thermal modulation of the plasma density in ionospheric heating experiments, J. Atmos. Terr. Phys., 44, 1049–1059, 1982.

Isham, B., Rietveld, M., Hagfors, T., LaHoz, C., Mishin, E., Kofman, W., and van Eyken, T. L. A.: Aspect angle dependence of HF enhanced ionospheric backscatter, Adv. Space Res., 24(8), 1003–1006, 1999.

Kosch, M. J., Pedersen, T., Hughes, J., Marshall, R., Gerken, E., Senior, A., Sentman, D., McCarrick, M., and Djuth, F. T.: Artificial optical emissions at HAARP for pump frequencies near the third and second electron gyro-harmonic, Ann. Geophys., 23, 1585–1592, 2005.

Minkoff, J. and Kreppel, R.: Spectral analysis and step response to radio frequency scattering from a heated ionospheric volume, J. Geophys. Res., 81, 2844–2856, 1976.

Mishin, E. V., Burke, W. J., and Pedersen, T.: On the onset of HF-induced airglow at HAARP, J. Geophys. Res., 109, A02305, doi:10.1029/2003JA010205, 2004.

Mishin, E. V., Kosch, M. J., Pedersen, T. R., and Burke, W. J.: HF-induced airglow at magnetic zenith: Thermal and parametric instabilities near electron gyroharmonics, Geophys. Res. Lett., 32, L23106, doi:10.1029/2005GL023864, 2005.

Noble, S. T.: Multiple-frequency radar observations of high-latitude *E* region irregularities in the HF modified ionosphere, J. Geophys. Res., 92, 13 613–13 627, 1987.

Pedersen, T., McCarrick, M., Gerken, E., Selcher, C., Sentman, D., and Gurevich, H. C. A.: Magnetic zenith enhancement of HF radio-induced airglow production at HAARP, Geophys. Res. Lett., 1169, doi:10.1029/2002GL016096, 2003.

Rietveld, M., Kosch, M., Blagoveshchenskaya, N., Kornienko, V., Leyser, T., and Yoeman, T.: Ionospheric electron heating, optical emissions and striations induced by powerful HF radio waves at high latitudes: Aspect angle dependence, J. Geophys. Res., 108, 1141, doi:10.1029/2002JA009543, 2003.

Robinson, T. R.: The heating of the high latitude ionosphere by high power radio waves, Phys. Rep., 179(2), 79–209, 1989.

Robinson, T. R., Honary, F., Stocker, A., and Jones, T. B.: Factors influencing the heating of the auroral electrojet by high power radio waves, Adv. Space Res., 15, 41–44, 1995.

Robinson, T. R., Bond, G., Eglitis, P., Honary, F., and Rietveld, M. T.: RF heating in a strong auroral electrojet, Adv. Space Res., 21, 689–692, 1998.

Robinson, T. R., Yeoman, T. K., Dhillon, R. S., Lester, M., Thomas, E. C., Thornhill, J. D., Wright, D. M., van Eyken, A. P., and McCrea, I.: First observations of SPEAR induced artificial backscatter from CUTLASS and the EISCAT Svalbard radar, Ann. Geophys., 24, 291–309, 2006.

Senior, A., Borisov, N. D., Kosch, M. J., Yeoman, T. K., Honary, F., and Rietveld, M. T.: Milti-frequency HF radar measurements of artificial F-region field-aligned irregularities, Ann. Geophys., 22, 3503–3511, 2004.

Stubbe, P., Kopka, H., Lauche, H., et al.: Ionospheric modification experiments in northern Scandanavia, J. Atmos. Terr. Phys., 44, 1025–1041, 1982.

Vas'kov, V. V. and Gurevich, A. V.: Nonlinear resonant instability of a plasma in the field of an ordinary electromagnetic wave, Sov. Phys. JETP, 42, 91–97, 1975 (engl. Transl.).

Vas'kov, V. V. and Gurevich, A. V.: Resonance instability of small-scale plasma perturbations, Sov. Phys. JETP Engl. Trans., 46, 487, 1977.

Yampolski, Y. M., Beley, V. S., Kascheev, S. B., Koloskov, A. V., Hysell, D. L., Isham, B., and Kelley, M. C.: Bistatic HF radar diagnostics of induced field-aligned irregularities, J. Geophys. Res., 102, 7461–7467, 1997.